Nondimensional Streaming Dielectrophoresis Number for a System of Continuous Particle Separation

Rucha Natu, Monsur Islam and Rodrigo Martinez-Duarte

Multiscale Manufacturing Laboratory, Department of Mechanical Engineering, Clemson University, Clemson, SC USA 29634

Supplementary information

S1. Table S1. Description of selected terms and variables used in this work

Symbol	Description
Design Parameters	
N	Number of columns in the electrode array
M	Number of rows in the electrode array
r_e	Radius of individual electrode in the array
C_x	Center to center distance between electrodes along X axis
C_y	Center to center distance between electrodes along Y axis
H	Channel height
w	Width of the channel
V	Voltage used to polarize electrodes
U_a	Magnitude of flow velocity in the channel before the electrode array, given by the ratio between the flow rate implemented Q and cross section area of the channel A
X_{in}	Location of particle entrance to the ROA*. Defined as the distance from this location to the center of the electrode in X axis along reference line AA
X_{stream}	Location of particle exit from the ROA*. Defined as the distance from this location to the center of electrode in X axis along reference line CC
$Re[f_{CM}]$	Real part of the Clausius Mossotti factor of the particle of interest. Depends on the difference between the dielectric properties of the particle and suspending media at a given frequency of the signal used to polarize the electrodes.
r_p	Radius of the particle of interest
Dependent/Auxiliary Parameters	
L	Length of the electrode array $L = NC_y$
X_{out}	Distance of particle from the center of the electrode along X axis at the last electrode in the array
K	Distance from the center of the last electrode to the reference line where streamwidth is measured
D	$d = C_x/2$
γ	Constriction ratio r_e/d
λ	Confinement ratio r_p/d
h	Height of the X-Y plane being analyzed, $0<h<H$
E	Electric field
$\vec{u}_p$	Particle velocity
$\vec{u}_{DEP}$	Particle velocity due to DEP force
u_{DEPx}	Magnitude of particle velocity due to DEP force in the X axis
u_{DEPy}	Magnitude of particle velocity due to DEP force in the Y axis
$\vec{U}_{flow}$	Flow velocity
U_{flowx}	Magnitude of flow velocity in the X axis
U_{flowy}	Magnitude of flow velocity in the Y axis
U_{avg}	Average velocity in the region between electrodes

*Note: some variables are rendered non-dimensional through division by d in the X axis, and L in the Y axis. Non-dimensional variables are denoted by an asterisk, i.e. $X_{in}^* = \frac{X_{in}}{d}$

S2. Relationship between $X_{out}{}^*$ and $X_{stream}{}^*$

X_{stream} is the final position of the particle along the line *CC* and it defines the distance at which the particle leaves the electrode array as shown in figure 1C. X_{out} is the particle position on line *BB*. The non-dimensional variables $X_{out}{}^*$and $X_{stream}{}^*$ are defined by dividing X_{out} and X_{stream} by d.

The positions $X_{out}{}^*$and $X_{stream}{}^*$ can be related by exploiting the ratio of the cross-sectional areas at *BB* and *CC* shown in figure 1C. All the particles that leave the reference line *BB* in the direction of the flow pass through the reference line *CC*. Thus, the flow of particles from the cross section $(d - r_e)H$ at reference line *BB*, expands into the region dH at reference line *CC*. As the particles travel from reference line *BB* to *CC*, the cross-sectional area increases, but the mass flux is conserved. Thus, the pathlines for particles spread out in the proportion of cross-sectional areas. Thus,

$$X_{stream}{}^* = \frac{(X_{out}{}^* - \gamma)}{(1-\gamma)} \qquad \text{(S1)}$$

where $\gamma = r_e/d$.

S3. Determining E^* using COMSOL Multiphysics:

Equation 8 in the main manuscript represents the best-fit curve to the computationally-modeled electric field in a domain of interest for various combinations of electrode radius r_e, distance between the electrodes d, constriction ratio $\gamma = r_e/d$ and polarization voltage V that are representative of experimental DEP devices in general. This approach follows from the work of previous authors [1,2] and consists of fitting a curve to the plot of the values of the average electric field for different conditions vs. their spatial location in the domain of interest. To this end, we first used the set of equations S2 to computationally model (COMSOL Multiphysics) the average E or E_{avg} along equidistant lines located across the domain of interest (see fig. S1A for examples) for different combinations of d, r_e and V. Stationary electric fields were used because the field frequency was smaller than the relaxation frequency for the current in the media used here and frequency does not have an effect on the charge density [3-5]

$$\nabla \cdot J = 0 \qquad \text{(S2)}$$
$$J = \sigma_m E$$
$$E = -\nabla V,$$ where J was the charge density and σ_m the media conductivity and

In our analysis we placed the equidistant lines 5 µm apart since a grid independence study (data not shown) illustrated how smaller gaps only led to a rate of change of electric field of 10% at most. Using computational modeling to derive E_{avg} and equation S3 to normalize E_{avg} against the parameters of interest in this work, a relation between the normalized field E^* and X^* was plotted as shown in figure S1B where $X^* = x/d$ and x was the distance in the X axis between a given equidistant line from the center of the electrode.

$$E^* = E_{avg}\left[\frac{(d-r_e)\sqrt{\gamma}}{V}\right] \qquad \text{(S3)}$$

The range of values for X^* reported is 0.1-1 since the minimum value of X^* is limited by the value of r_e/d and its maximum by d/d. The best fit curve to the results in figure S1B is reported by equation S4 and was obtained by using inverse curve fit. This fit, with R=0.95, was chosen because the electric field magnitude is inversely proportional to the distance of the particle to the electrode. Equation S4 represents the average electric field depending on the distance of the particle from the electrode as well as on the electrode radius.

$$E^* = 0.55\left(\frac{X^*}{\gamma}\right)^{-1} \qquad \text{(S4)}$$

Equation S4 only considers the effect of the electric field between two neighboring electrodes since the influence of those electrodes located diagonal to the studied electrodes in the streamingDEP device is small. However, this equation will show deviations if the distance between electrodes decreases and the diagonal electrodes make significant contribution to the field. Such variations are pending to be determined in future work. Envisioned work also includes a non-dimensional relaxation factor to capture the effect of frequency in the electric field.

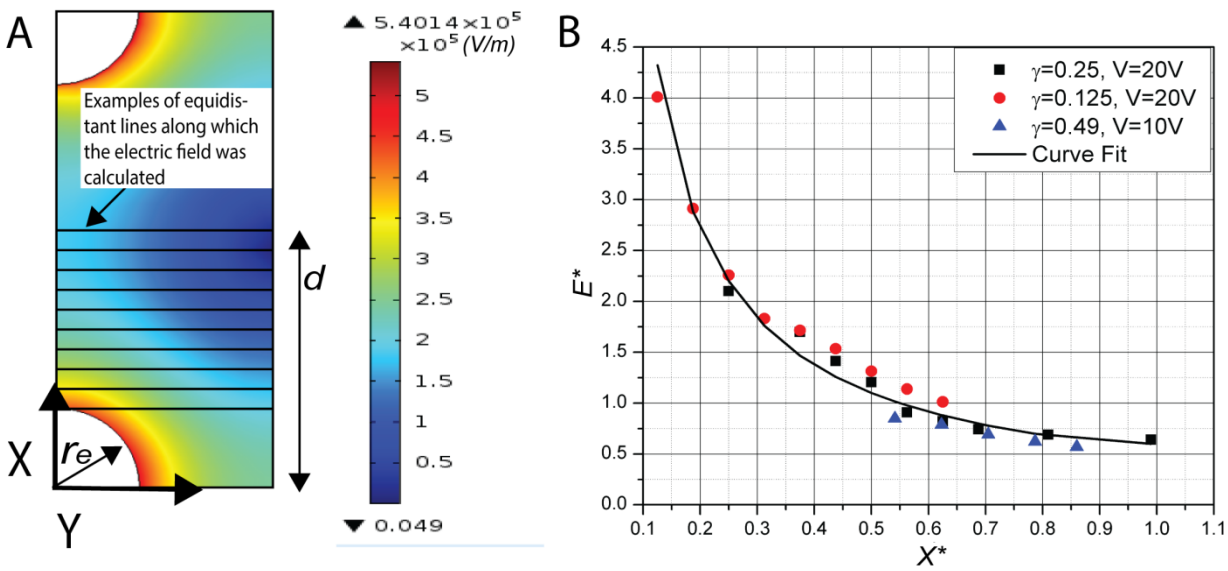

Figure S1 A) Domain of interest between the electrodes where the electric field was modeled for different combinations of electrode radius r_e, distance between the electrodes d, constriction ratio $\gamma = r_e/d$ and polarization voltage V that are representative of experimental DEP devices in general. Using computational modeling, the average electric field E_{avg} was calculated on each of the horizontal lines. B) Points in the graph denote E^* as calculated using equation S3 depending on X^* for three representative combinations of V and γ. Solid line represents the best fit curve to the data average values, R=0.95.

S4. Comparison between U_{flowy} and u_{DEPy} along the Y axis

The magnitude of the particle velocity in the y direction u_{py} is the sum of u_{DEPy} and U_{flowy} in the domain. These two components were computed along the line joining the electrodes along the X axis, as shown in figure S2A, for the case of highest voltage (20 V), or strongest DEP force, and lowest flow velocity used in this work (0.015 m/s). Results are shown in figure S2B relating u_{DEPy} and U_{flowy} to the distance from the particle to the electrode center at the entrance of the ROA (reference line *AA*) given by X_{in}. The results in figure S2B are shown for electrodes with radius 20 µm and hence the $X_{in} > 20$. Close to the electrodes, the DEP velocity is high but rapidly decreases as the distance from the electrode increases. Inversely, the flow velocity rapidly increases as one moves away from the electrode. Regardless, u_{DEPy} is at least 10^3 times smaller than U_{flowy}. This relation is expected to be valid in the devices used for streamingDEP of particles with diameter above hundreds of nanometers. The effect of u_{DEPy} will only become a competing factor to U_{flowy} if the gap between the electrodes decreases to below few micrometers.

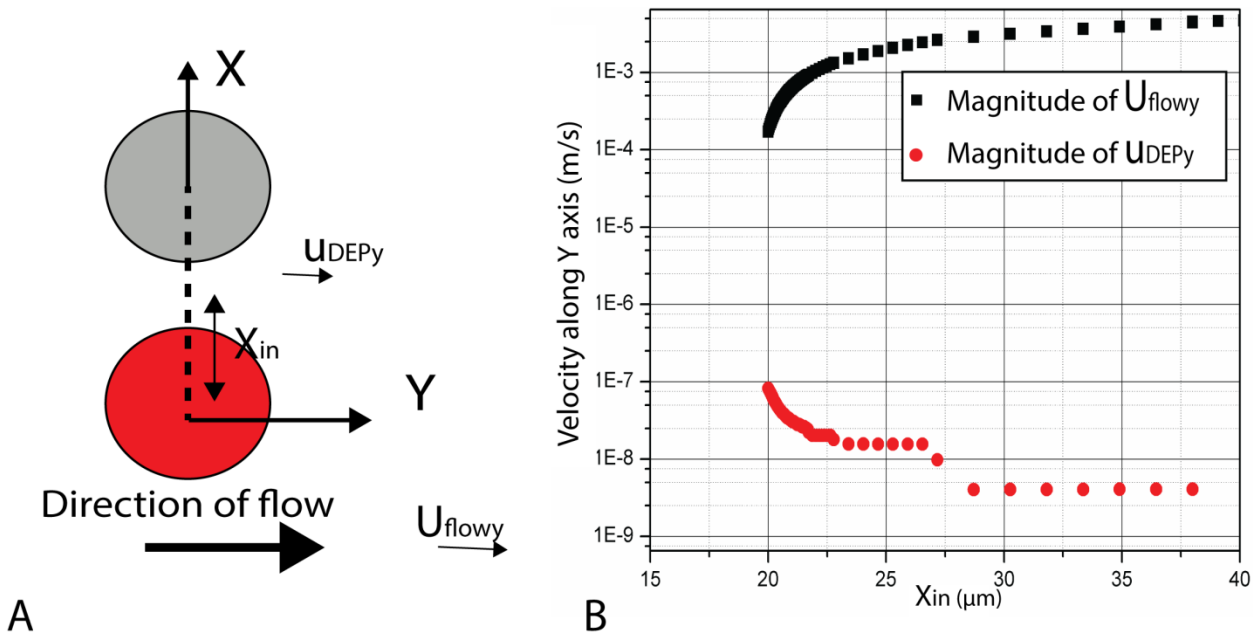

Figure S2. A) Domain analyzed. U_{flowy} and u_{DEPy} were analyzed in the dashed line connecting both electrodes in the X axis. B) The comparison of magnitude of u_{DEPy} and U_{flowy}. The velocity magnitude due to the flow is at least 10^3 times higher than that due to DEP force.

S5. Calculation of U_{flowy} in the ROA

The flow profile in a microfluidic device featuring post arrays was previously reported to be of a 3D parabolic nature [6]. Equation 11 in the manuscript describes the flow profile in the narrowest gap between electrodes in the array at a given X-Y plane located at height *h* from the bottom of the channel in function of device design parameters U_a, or velocity in the channel, and *H*, or height of the channel. Towards defining equation 11, we first derived an analytical expression for the average magnitude of the flow velocity in the channel in a X-Y plane at height *h*. To this end, we obtained the maximum velocity magnitude at a given *h* by analyzing the Y-Z plane in the center of the channel and considering a flow between two stationary parallel plates, the channel floor and ceiling. This flow is well described by the parabolic equation S5 for the case of water-based media [7-9].

$$U_h = 6U_a\left(\frac{h}{H}\right)\left(1-\frac{h}{H}\right) \qquad \text{(S5)}$$

Where U_a is the average velocity in the channel prior to the electrode array and can be calculated from equation S6,

$$Q = U_a A \qquad \text{(S6)}$$

Where Q is the volume flux in the channel (in m^3/s) and A is the cross-sectional area of the channel (in m^2). Once the maximum velocity U_h at *h* was obtained, the average magnitude of flow velocity in the X-Y plane at *h* was determined using equation S7 by considering that the average velocity magnitude in a parabolic profile is 2/3 times its maximum velocity,

$$U_{ah} = \left(\frac{2}{3}\right)U_h = 4U_a(h/H)\left(1-\frac{h}{H}\right) \qquad \text{(S7)}$$

Second, we derived an expression for U_{flowy} in the ROA as flow between two stationary boundaries, the electrodes, in the X-Y plane at a given height *h* and in function of the location of particle flow between the electrodes (X_{in}-r_e) and the narrowest gap between electrodes ($C_x - 2r_e$) or $2(d - r_e)$. Equation S5 was thus modified to replace h by ($X_{in} - r_e$); H by $2(d - r_e)$; and U_a by the term U_{avg}, or the average velocity in the narrowest gap between electrodes, to obtain equation S8,

$$U_{flowy} = 6U_{avg}\left(\frac{X_{in}-r_e}{2(d-r_e)}\right)\left(1-\frac{(X_{in}-r_e)}{2(d-r_e)}\right) \qquad \text{(S8)}$$

And on normalizing the terms in equation S8 by dividing by d and rearranging them,

$$U_{flowy} = \frac{6U_{avg}(X_{in}{}^{*}-\gamma)(2-\gamma-X_{in}{}^{*})}{(1-\gamma)^2} \qquad \text{(S9)}$$

Where U_{avg} was determined by relating U_{ah} and U_{avg} using the continuity equation and considering a constant H. Since the flux in the channel must be similar to the flux flowing through the electrode array,

$$Q_{channel} = Q_{array} = wU_{ah} = U_{avg}[2(d-r_e)(M-1)+2(d-r_e)] = 2(d-r_e)U_{avg}M \qquad \text{(S10)}$$

Where w is the width of the channel, M is the number of electrode rows, and the distance between the outer electrodes in the array and the channel boundary was assumed to be $(d-r_e)$.

On combining equations S5-S10, the final equation for U_{flowy} is thus given as;

$$U_{flowy} = \frac{12U_a(h/H)(1-h/H)(w/d)(X_{in}{}^{*}-\gamma)(2-\gamma-X_{in}{}^{*})}{M(1-\gamma)^3} \qquad \text{(S11)}$$

S.6 Clausius Mossotti Factor for latex particles

The real part of Clausius Mossotti factor $Re[f_{CM}]$ for 1 µm latex particles and *S. cerevisiae* cells was obtained for the frequency range 10^3-10^9 Hz using models previously reported by multiple authors [10-13]. Results are shown in Figure S3A for latex particles. For the case of *S.cerevisiae*, results are shown in figure S3B. System properties used to calculate the $Re[f_{CM}]$ values are shown in Table S2.

Table S2. Properties used to compute the Re[fcm] values for latex particles [10,11] and S.cerevisiae cells [12-14]

Parameter	**Value**
Latex Particles	
Diameter	1 µm
Media conductivity	10^{-5} S/m
Conductivity of particles	$5.2*10^{-3}$ S/m
Surface conductance of particles	$1.3*10^{-9}$ S
***S.cerevisiae* cells**	
Diameter	4 µm
Media conductivity	$2*10^{-3}$ S/m
Relative permittivity of cell wall	60
Relative permittivity of membrane	6
Relative permittivity of cell interior	50
Membrane thickness	8 nm
Thickness of cell wall	0.22 µm
Conductivity of cell wall	$1.4*10^{-3}$ S/m
Conductivity of cell membrane	0.25 µS/m
Conductivity of cell interior	0.2 S/m

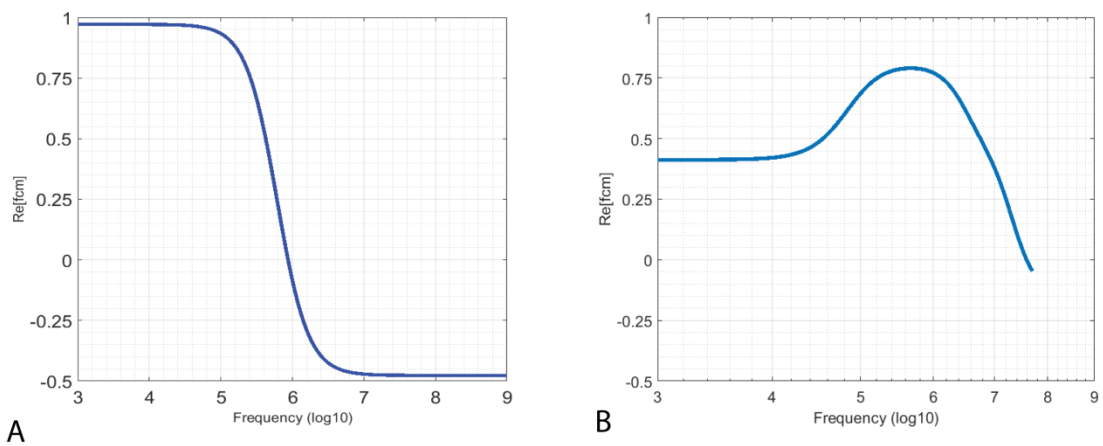

Figure S3. A) The $Re[f_{CM}]$ value for 1µm latex particles used in this work. B) The $Re[f_{CM}]$ value for *S.cerevisiae* cells is used to represent *C.albicans* cells in this work. See main manuscript for details.

References:

[1] J.G. Kralj, M.T.W. Lis, M.A. Schmidt, K.F. Jensen, Continuous dielectrophoretic size-based particle sorting, Anal. Chem. 78 (2006) 5019–5025.

[2] T. Schnelle, T. Muller, G. Gradl, S.G. Shirley, G. Fuhr, Paired microelectrode system: dielectrophoretic particle sorting and force calibration, J. Electrostat. 47 (1999) 121–132.

[3] A. Kale, S. Patel, G. Hu, X. Xuan, Numerical modeling of Joule heating effects in insulator-based dielectrophoresis microdevices, (2013) 674–683.

[4] A. Ramos, H. Morgan, N.G. Green, A. Castellanos, Ac electrokinetics: a review of forces in microelectrode structures, J. Phys. D. Appl. Phys. 31 (1998) 2338–2353.

[5] A. Castellanos, A. Ramos, A. González, N.G. Green, H. Morgan, Electrohydrodynamics and dielectrophoresis

in microsystems: scaling laws, J. Phys. D. Appl. Phys. 36 (2003) 2584–2597.

[6] R. Martinez-Duarte, S. Cito, E. Collado-Arredondo, S.O. Martinez, M.J. Madou, Fluido-dynamic and Electromagnetic Characterization of 3D Carbon Dielectrophoresis with Finite Element Analysis, Sensors Transducers J. 3 (2008) 25–36.

[7] Y. Huang, X.B. Wang, F.F. Becker, P.R.C. Gascoyne, Introducing dielectrophoresis as a new force field for field-flow fractionation, Biophys. J. 73 (1997) 1118–1129.

[8] J. Yang, Y. Huang, X.B. Wang, F.F. Becker, P.R.C. Gascoyne, Cell separation on microfabricated electrodes using dielectrophoretic/gravitational field flow fractionation, Anal. Chem. 71 (1999) 911–918.

[9] P.R.C. Gascoyne, J. Vykoukal, Particle separation by dielectrophoresis, Electrophoresis. 23 (2002) 1973–1983.

[10] I. Ermolina, H. Morgan, The electrokinetic properties of latex particles: comparison of electrophoresis and dielectrophoresis, J. Colloid Interface Sci. 285 (2005) 419-428.

[11] M.P. Hughes, Dielectrophoretic behavior of latex nanospheres: Low-frequency dispersion, J. Colloid Interface Sci. 250 (2002) 291–294.

[12] Z.R. Gagnon, Cellular dielectrophoresis: Applications to the characterization, manipulation, separation and patterning of cells, Electrophoresis. 32 (2011) 2466–2487.

[13] Y. Huang, R. Hölzel, R. Pethig, X.B. Wang, Differences in the AC electrodynamics of viable and non-viable yeast cells determined through combined dielectrophoresis and electrorotation studies., Phys. Med. Biol. 37 (1992) 1499–1517.

[14] R. Martinez-Duarte, Label-free Cell Sorting using Carbon-electrode Dielectrophoresis and Centrifugal Microfluidics, University of California, Irvine, 2010.